Construction and Building Materials 260 (2020) 119948

Contents lists available at ScienceDirect

Construction and Building Materials

journal homepage: www.elsevier.com/locate/conbuildmat

Electrically conductive concrete: A laboratory-based investigation and numerical analysis approach

Heydar Dehghanpour [a], Kemalettin Yilmaz [a], Faraz Afshari [b,*], Metin Ipek [c]

[a] Sakarya University, Engineering Faculty, Civil Engineering Department, 54187 Sakarya, Turkey
[b] Erzurum Technical University, Department of Mechanical Engineering, 25240, Erzurum, Turkey
[c] Sakarya Applied Sciences University, Technology Faculty, Civil Engineering Department, 54187 Sakarya, Turkey

HIGHLIGHTS

- Different ECON mixtures were produced.
- The mechanical and electrical properties of the specimens were examined.
- Electrothermal analysis of specimens were made: experimental and numerical.
- NCB was found to be favorable material considering basic and electrodermal test results.
- N6C1S0 specimen was selected as proper production by optimization process.

ARTICLE INFO

Article history:
Received 23 March 2020
Received in revised form 7 June 2020
Accepted 10 June 2020

Keywords:
Electrically conductive concrete
Anti-icing
Carbon fiber
Nano carbon black
Wire erosion

ABSTRACT

In recent years, the application of electrically conductive concretes has been proposed as an anti-icing method on airport runways. In this work, it was aimed to evaluate usability of the nano carbon black obtained by the pyrolysis method from the waste tires and also the waste wire erosion obtained from the cutting processes for using in the electrically conductive concrete with application in airport runway anti-icing. In this regard, 36 different mixtures of the electrical conductive concretes were first investigated in the laboratory to find out general mechanical and electrical conductivity properties of the test concrete. After obtaining the result of their general characteristics, 10 different types of concrete slabs were produced. Electrothermal tests of conductive concrete slabs were carried out in a cooling chamber at −10 °C. A heat power within a range of 180–1315 W/m^2 has been provided for heating electrically conductive concrete slabs obtained from different mixtures and consequently an optimization method was utilized and obtained results were compared on figures and diagrams. Numerical simulation of the problem has been also carried out to find out heat flux and temperature distribution of test concretes.

1. Introduction

In cold regions, the formation of snow and ice on the road surfaces causes infrastructure deterioration and damages the concrete coating. In order to avoid such an event, spraying chemical substances on the road pavement and using traditional defrosting methods would lead to negative environmental impacts [1–3]. Heated paving systems are one of the alternative options for melting ice and snow. These systems can be divided into two general groups including hydronically heated paving systems [4] and electrically heated paving systems [5,6].

Hydronically heated paving systems melt the ice and snow by passing the heated fluid through pipes embedded in road pavement structures. The cooled fluid recirculates in a heat source which heats during each cycle. There are different types of heat sources including geothermal water, boilers and heat exchangers. In electrical systems, melting of snow and ice takes place through resistive heating of electrically conductive cables embedded in conventional concrete or through using an electrically conductive concrete capable of resistive heating. Due to the high power density required, the performance of the resistance cables is sometimes inadequate and the equipment and systems connected to it are damaged [1,7]. Also, these cables will produce localized hot regions that can be detrimental. In recent years, the use of ECON-

* Corresponding author.
E-mail addresses: heydar.dehghanpour@ogr.sakarya.edu.tr (H. Dehghanpour), kmyilmaz@sakarya.edu.tr (K. Yilmaz), faraz.afshari@erzurum.edu.tr (F. Afshari), metini@sakarya.edu.tr (M. Ipek).

https://doi.org/10.1016/j.conbuildmat.2020.119948
0950-0618/

Nomenclature

AI	Fine aggregate
AII	Coarse aggregate
ASTM	American Society for Testing and Materials
ASTM-D	Resistance measured by ASTM method
BM	Bulk method
CNT	Carbon nanotube
Cp	Heat capacity (J kg^{-1} K^{-1})
CEA	Conductivity-enhancing agent
C/F	Coarse/fine
CF	Carbon fiber
CMS	Carboxymethyl cellulose
e	Energy (J)
E	Electrical field (V m^{-1})
EA_u	Absorbed final energy (J)
ECON	Electrically conductive concrete
EDS	Energy dispersive spectrometer
EHPS	Electrically heated paving systems
E_U	Final impact energy (J)
g	Gravity (m s^{-2})
h	Height (m)
I	Electric current (A)
J	Electric current density (A m^{-2})
k	Coefficient of thermal conductivity ($Wm^{-1}K^{-1}$)
L	Length (m)
m	Mass (kg)
N_u	Impact number
NCB	Nano carbon black
P	Power (W m^2)
Q	Heat transfer (W m^{-3})
r_c	Internal volumetric current (A m^{-3})
R	Electrical resistance (Ω)
SEM	Scanning electron microscope
SP	Superplasticizer
t	Time (s)
T	Temperature (°C)
TEM	Tunneling electron microscope
V	Voltage (V)
WPM	Wenner prop method
WWE	Waste wire erosion
ρ	Resistivity (Ω.cm)
σ	Electrical conductivity (S m^{-1})
σ_c	Compressive strength (MPa)
σ_f	Flexural strength (MPa)

based heated paving systems has also attracted researcher's attention to reduce the problems of ice and snow accumulation in highways and airports. Electrically conductive concrete (ECON) works by applying voltage to the embedded electrodes to melt ice and snow. The electrical conductivity and mechanical properties of steel fiber, carbon fiber and other conductive materials of ECONs have been investigated widely in literature in different studies [3,8–11].

ECONs are used as a self-sensing material for monitoring the health of structure [12,13], as a strain/stress sensor [14], as an electromagnetic radiation reflector for electromagnetic interference shielding, and as resistance material in heated pavement [15–18]. This type of heated pavement has recently been applied to melt snow and ice on road and airport runways [19–21]. It has been confirmed by different research that electrical resistivity of concrete is at high levels. Electrical resistivity of outdoor dried concrete was determined as 6.54×10^5–11.4×10^5 Ω-cm [22]. In addition, the electrical resistivity of saturated concrete and dry concrete was reported to be 10^6 Ω-cm and 10^9 Ω-cm, respectively, according to research conducted by different researchers [23,24]. Carbon fiber is a material used and tested as an electrically conductive additive in the production of electrically conductive cementitious composites for different purposes. In addition, carbon fiber reinforced concrete has been found to be physically and mechanically resistant material from previous studies [25–27]. In carbon fiber doped concrete, not only the carbon fiber content, but also its length, mixing method and dispersion are important factors affecting the conductivity. In many research, powdered methyl cellulose admixture has been used to ensure the distribution of carbon fiber in concrete [28]. According to some research results, differences between electrical resistivity results measured by various methods have been reported [29–34]. Ghosh et al. compared the electrical resistivity of high performance cylinderical concrete specimens with different mixtures by measuring with two different methods including bulk and surface electrical resistivity measurement methods. According to the results, the ratio of total electrical resistance value to surface resistance value was calculated between 0.29 and 0.49 for different mixtures [33]. The authors of the present study have found this ratio to be about 0.25 in previous study available in the literature [34].

The aim of this study is to produce electrically conductive concrete to use for melting the ice and snow accumulated on airport runways in cold regions. Specific tests of produced concrete have been carried out by taking advantage of the mechanical, electrical and thermal properties of the prıposed materials as well as the economic factor. In this regard, it was aimed to produce a durable concrete capable of anti-icing on airport runways, and also to use the nano carbon black in the produced concrete by recycling the waste tires for making concrete runway more compatible with the winter conditions in Turkey's airports.

2. Experimental setup and test procedure

2.1. Materials

Two different aggregates including coarse-grained and fine-grained, were used for ECON mixtures. The amount of water and sedimentation value of the mixture, grain distribution and maximum grain size were selected in accordance with TS802 [35] standard. Materials properties used in this study are given as follows,

2.1.1. Cement

ECON is an engineered material designed for certain applications. For example, its resistive heating feature can be utilized for keeping the airfields free of ice and snow, so that the airport operations would not be interrupted. According to previous studies, the type of this concrete is designed on C35-C40 class. For this purpose, over 400 kg high strength cements should be used for 1 m^3 of concrete [36]. Hence, 42.5 CEM I R type high strength cement was preferred in this study. The EDS analysis results of the used cement are given in Table 1.

2.1.2. Aggregates

Two different crushed aggregate types with a grain size range of 0–4.75 and 4.75–22 mm were used. Table 2 shows the gradation of coarse and fine aggregates. Coarse aggregates (4.75–22 mm) used

Table 1
EDS Analysis results of cement.

Elt.	Line	Intensity (c/s)	Error 2-sig	Conc	Units	
C	Ka	0.06	0.156	0.048	wt.%	
O	Ka	14.29	2.390	25.508	wt.%	
Al	Ka	7.75	1.760	1.192	wt.%	
Si	Ka	89.23	5.972	11.860	wt.%	
K	Ka	2.66	1.030	0.321	wt.%	
Ca	Ka	407.91	12.768	59.666	wt.%	
Fe	Ka	4.65	1.363	1.405	wt.%	
				100.000	wt.%	Total

Table 2
Gradation of coarse and fine aggregates.

Coarse aggregate		Fine aggregate	
Sieve size (mm)	Cumulative retained (wt.%)	Sieve size (mm)	Cumulative retained (wt.%)
20	0	4.75	0
16	17	2.36	18
12.5	62	0.60	43
10	78	0.30	79
4.75	100	0.15	91
		<0.15	100

in the study are calcium carbonate origin aggregates obtained from rocks and fine (0–4.75 mm) aggregates are silica origin aggregates. These Aggregates with this mineralogical structure are widely used in concrete production in Turkey.

2.1.3. Carbon fiber (CF)

In this study, CF was used as the most effective electrical additive in three different ratios, 0.2%, 0.5% and 1 vol% relative to the total mixture volume. In order to facilitate the distribution of the fibers in the concrete mixture, carboxymethyl cellulose was used as the dispersing additive. According to literature, when carbon fiber is used at high rates such as more than 0.75 vol%, a concrete mixture with a water-cement ratio of 0.45 shows normal workability [37]. The used carbon fiber has a filament diameter of 7.2 μm and a length of 6 mm and 12 mm in equal proportions.

2.1.4. Nano carbon black (NCB)

Having high electrical conductivity, NCB is often used to produce electrically conductive composite materials. In recent years NCB has also been used in cementitious materials for different purposes [38–42]. On the other hand, carbon black can be obtained in large volume by recycling waste tires as polluting material by using pyrolysis process. The effect of NCB on strength of concrete was investigated by Norouzi and according to the results of using this nano material in different ratios, concrete specimens containing 4 wt% nano carbon showed maximum compressive strength [44]. Therefore, there is not a problem in terms of strength due to using this material in the mixture. In this study, nano carbon black obtained by pyrolysis method was used in 4 different ratios as 0%, 3%, 6% and 10 wt% according to the weight of binder. The specific surface area of the nano carbon black can be increased up to 88 m^2/g by increasing the applied temperature to 600 °C during production [43]. The obtained carbon black is between N200-N330 according to ASTM nomenclature [44].

It has been proven that, in different insulation matrices, carbon fiber has percolation threshold [45–47]. In addition, the authors have proven that, NCB percolation threshold is increased in their previous study [34]. Percolation theory provides an idea regarding the minimum amount of conducting filler required for converting an insulating matrix to a conducting one [45].

Fig. 1, shows a schematic view of the internal structure of the conventional and electrically conductive concrete. Fig. 1-a is normal concrete containing only aggregate and cement, and isn't electrically conductive material. Carbon based fiber materials are used to provide the electrical conductivity of cement based materials (Fig. 1-b). The fiber randomly settles between the aggregates to form a complex network and acts as a bridge for electric current. Cement paste is defined as a matrix element for fibers between aggregates. If the cement paste is combined with conductive materials in powder form, it is expected that the electrical conductivity of fibers will increase. As shown in Fig. 1-c., the powdered carbon black filled the inter-granular spaces and so the interface area between the fiber and the matrix increased.

2.1.5. Waste wire erosion (WWE)

Wire erosion is a conductive wire used to cut a workpiece in electrical discharge processing and widely used in CNC devices. The cutting wire moves at a close distance without direct contact with the workpiece, and is eroded over time and stored as waste product. In this study, yellow CuZn37 alloy WWE with a diameter of 0.25 mm and an average length of 25 mm was used. The electrical resistance of WWE is measured as 0.00256 Ω-cm.

2.1.6. Steel fiber (SF)

SF was used as conductive additive material in the early ages of the production of conductive concrete. When the SF is present in the alkaline medium in concrete, a passive film is formed, which increases the electrical resistance over time which cause to a decrease the resistance of electrically conductive of concrete 60 times after one year. Therefore, it is not appropriate to use SF alone in conductive concrete [19]. Steel fiber can be used in different ratio as presented in the literature. In this study, 30 mm length, 0.75 mm diameter and 1400 MPa tensile strength SF have been used.

2.1.7. Chemical additives

In the case of using small diameter CF and small grain carbon black in the concrete mixture, more water is needed due to the high specific surface area of the materials. In order to reduce the amount of water, a plasticizer chemical liquid with the trade name MasterGlenium SKY4123 has been used. MasterGlenium is a superplasticizer used for high strength concrete containing different powder additives [48–50]. A variety of chemicals can be used to facilitate the distribution of fibers in the concrete mixture. It has been specified that methyl cellulose in small dosages is an effective fiber dispersing material [18,51,52]. In this study, 0.2% carboxymethyl cellulose (CMC) was used as fiber distributor according to the weight of cement. The authors have used the carboxymethyl cellulose in their previous works in [34,53,54] and have proved carboxymethyl cellulose to be a fiber distributor.

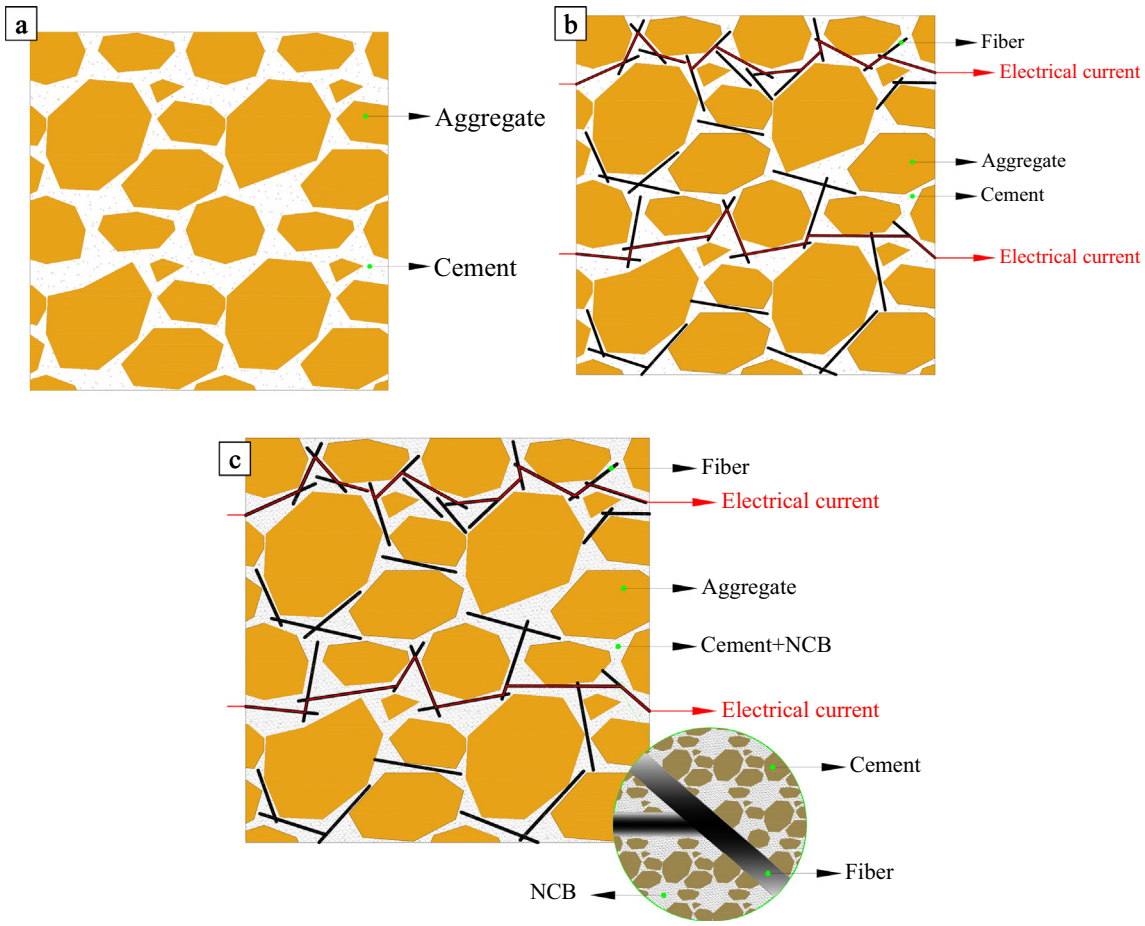

Fig. 1. Schematic view of the internal structure of (a) conventional concrete, (b) fiber doped concrete, and (c) fiber and NCB doped concrete"

2.2. Mixture design

The aim of this study is to optimize 36 different mixtures and perform both simulation and experimental electrothermal experiments on mixtures. The optimum amount of CF used in electrically conductive concretes was found to be 0.75–1 vol% according to the studies in the literature. However, since there was no previous study on the combined use of CF and nano carbon black, it was aimed to obtain the optimum amount of CF and carbon black using 4 different ratios of CF and 4 different ratios of carbon black in electrically conductive concrete mixtures. Because of containing 0 and 2 wt% steel fiber, mixtures are composed in 2 groups. In all mixtures, gravel: sand: cement ratio was taken as constant 1: 1: 0.5. In the mixtures, the water/binder ratio was constant at 0.45 and a superplasticizer additive was used as a variable to improve workability. In this research, the slump of normal concrete mixture was 80 mm and decreased to approximately 40 mm with the addition of filling materials. Slump values for the all mixtures are given in Table 3. The acceptability of slump values has been confirmed for ECON from Sassani's study [18]. A slight segregation requirement was experienced in the mixture with 1% CF ratio. This problem was not observed in mixtures containing different ratios of NCB having the same mixture. The results of the specimens containing CF and NCB produced in the first stage of the study were obtained and then WWE-containing specimens were produced at the same size in 4 different mixture ratios. In all 4 mixtures, constant weight ratio (%6) of NCB and different ratios of CF and WWE were used.

2.3. Basic test methods

The compressive and flexural strengths of the electrically conductive concrete have been tested mechanically by universal laboratory test equipment with 250 tons and 5 tons capacity respectively. In the present study, the ECON mixtures are designed for use on airport runways. The runway concrete is exposed to the impact when the aircraft is seated at the airport. Therefore, it is also important to examine the produced concrete against impact. In order to perform the impact test, the impact test device designed in the laboratory was used. In the experiment, the slab specimen is placed on a square support at the bottom of the instrument. A mass of 1.1 kg falls freely from a height of 45 cm into the center of the specimen, and the impact test is performed. Experiments was continued until the final crack in the specimen was formed. The final energy value was calculated using the multiplication number of test as [55,56],

$$e = m \times g \times h \tag{1}$$

$$EAu = Nu \times e \tag{2}$$

where EAu is the final absorbed energy.

The resistance of electrically conductive concrete can be measured by different methods [54].

1. Two-point uniaxial method or bulk method: in this method, a certain potential difference between the two surfaces of the specimen is applied. The electrical current between the two

Table 3
Mixture details in electrothermal test specimens – for 1 m^3, N: Nano carbon black, C: Carbon fiber, S: Steel fiber, E: WWE.

No	Mixing Code	AI (kg)	AII (kg)	Cement (kg)	Water (kg)	SF (wt%)	WWE (kg)	NCB (kg)	CF (kg)	CMS (wt%)	SA (wt%)	Slump (mm)
1	N10C0.2S0	831.56	831.56	415.78	206.23	0.00	0.00	42.50	3.60	0.20	1.00	65
2	N6C0.5S0	836.23	836.23	418.12	199.63	0.00	0.00	25.5	9.00	0.20	1.50	60
3	N6C1S0	832.58	832.58	416.29	198.81	0.00	0.00	25.5	18.00	0.00	1.75	45
4	N10C0.2S2	812.77	812.77	406.39	202.00	2.00	0.00	42.50	3.60	0.00	1.00	65
5	N6C0.5S2	817.36	817.36	408.68	195.38	2.00	0.00	25.5	9.00	0.00	1.50	55
6	N6C1S2	813.79	813.79	406.90	194.58	2.00	0.00	25.5	18.00	0.00	1.75	40
7	N6 C0E0.5	822.80	822.80	411.40	196.61	0.00	42.50	25.5	0.00	0.20	0.75	70
8	N6 C0E1.0	805.80	805.80	402.90	192.78	0.00	85.00	25.5	0.00	0.20	0.75	60
9	N6C0.2E1.0	804.36	804.36	402.18	192.46	0.00	85.00	25.5	3.60	0.20	1.6	50
10	N6C0.2E1.5	787.36	787.36	393.68	188.63	0.00	127.5	25.5	3.60	0.20	1.6	45

surfaces of the specimen is measured as a result of the applied voltage. Using the Ohm's law, the electrical resistance of the specimen is calculated as.

$$V = I.R \tag{3}$$

2. Four-probe or Wenner probe method (WPM): in this method, the resistance measurement is performed by applying voltage to the four-probe equipment which is contacted with the surface of a cylinder specimen. By applying a certain potential difference between the two internal probes, the amount of current flowing between the two external probes is measured. Resistance is calculated from Ohm's law and the surface resistivity of the specimen is obtained as,

$$\rho = 2.\pi.a.R \tag{4}$$

where ρ is the electrical resistivity, a is the distance between the probes and R is the electrical resistance of the specimen.

3. C1760-12 ASTM method: In this method, the electrical resistance of the specimens is measured with the device in accordance with ASTM C1760-12 standards. According to C1760-12, the test is carried out by measuring the amount of current flowing through the concrete specimen placed in solution containing sodium chloride on both surfaces within 1 min.

In this study, all three methods were used to measure resistance of electrically conductive concrete. The resistance of conductive concrete can be measured using alternating current (AC) or direct current (DC). In the study of Abdualla to supply electrothermal power to ECON, AC current is suggested to be more suitable because uniform heat is generated with this type of current [1]. AC current was used throughout the measurement in the present study.

2.4. Electrothermal test method

According to the electrical conductivity results obtained from the previous study [34], 10 mixtures of 36 mixtures were selected for electrothermal tests (Table 3). From the selected mixtures 10 equal sized 45 × 45 × 5 cm slab specimens were produced. 45 mm × 5 cm stainless galvanized steel sheet was used as electrode. In order to ensure the adhesion between the slabs and the concrete in the produced slab specimens, screws with a diameter of 3 mm with a depth of 5 cm in each 6 cm intervals were used.

Because of the low resistivity values of N10C0.2S0, N10C0.2S2, N6C0.5S0, N6C0.5S2, N6C0E0.5, N6C0E1 slab specimens, four different voltages were applied as 100, 140, 180 and 220 V. The thermal behavior of a slab specimens N6C1S0, N6C1S2, N6C0.2E1, N6C0.2E1.5 ECON were investigated by applying four different voltages of 60, 80, 100 and 120 V due to their high resistivity. The initial temperatures of all specimens were adjusted to −10° C according to the capacity of the refrigerator, and the refrigerant was also operated from the beginning to the end of the experiments.

For the compressive strength and electrical resistivity measurement tests of the electrically conductive concrete, cylindrical specimen molds with a diameter of 10 cm and a height of 20 cm were used. For the flexural test of all mixtures, prismatic specimens of 10 × 10 × 40 cm were used. For the impact test, since there is no special specimen mold for the concrete slabs, 10 × 10 × 10 cm cube specimen molds were used and a 3 cm thick concrete mixture was filled to the bottom of the molds and they are compressed under the same conditions of compression of the other molds.

All specimens were removed from the molds after 24 h and were cured in the curing pool over 7 days (Fig. 2a). Since the top of the cylindrical specimens were rough, they were cut 1 cm from the tops. In Sassani's [18] study all specimens were cured at 100% relative humidity and 23 °C temperature during the entire study. In the current study all specimens were kept in laboratory condition for drying at room temperature during the entire study (Fig. 2b). Since the resistance of moist concrete is lower than dry concrete [23,24], this study aimed to measure the maximum resistance in the most critical condition of concrete (dry).

In order to monitor the temperature changes of the specimens inside the refrigerator during the experiments, 9 equal intervals holes were drilled 5 mm deep on the slab surfaces and with the diameter of 4 mm according to thermocouple thickness (Fig. 3-a). The specimens were placed one by one in the refrigerator on the wooden bases, and the metal parts at the ends of the thermocouples were mounted in the holes. The wood used in the experimental setup is to provide insulation between the specimen and the refrigerator and to prevent any current.

As shown in Fig. 3-b, electrothermal tests were carried out by applying different voltages using an adjustable power source between the electrodes made of stainless steel sheet located on both sides of the slab specimen and the amount of current was recorded during the tests. The obtained current values were used as the second model in the electrothermal analysis of slab specimens and used in temperature-resistivity curves for 10 different specimens. The appropriate voltages were selected considering literature studies by making a preliminary power consumption calculation, resistivity values and first model results in order to prevent loss of time during the experiment.

The electrical resistance of ECON is the reason for the conversion of electrical energy to thermal energy. A transient model of heat conduction can be used to predict the change of temperature

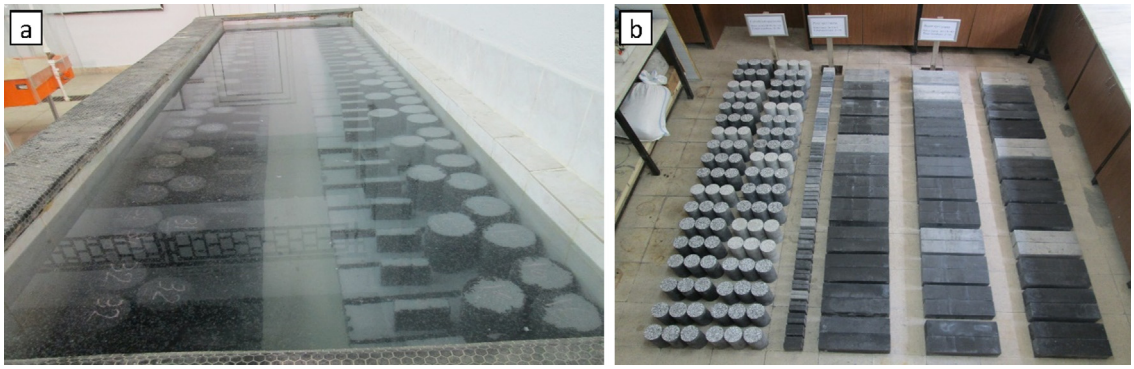

Fig. 2. a) Placement of specimens in curing pool, b) Drying the specimens at room temperature.

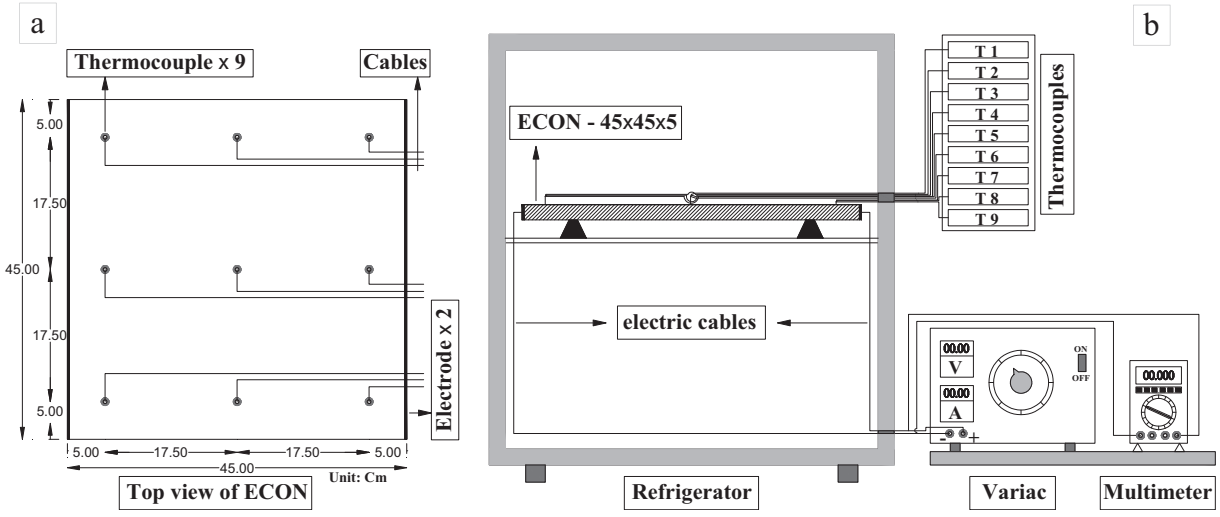

Fig. 3. Thermocouples configuration a) schematic view of the refrigerator b).

as a function of time, material specifications in an ECON specimen. Three-dimensional mathematical model for transient heat conduction is expressed by [57],

$$\dot{Q} = \rho C \frac{\partial T}{\partial t} - \nabla.(k \nabla T) \tag{5}$$

where $\dot{Q}$ is heat generated per m^3.

In the case of constant conductivity,

$$\frac{\dot{Q}}{k} = \frac{1}{\alpha}\frac{\partial T}{\partial t} - \nabla.(\nabla T) \tag{6}$$

where α is heat diffusion coefficient and equals to $(k/\rho c)$.

Energy balance can be also expressed using convection heat flux where thermal energy is transferred from ECON slab surface to the atmosphere ambient as,

$$\boldsymbol{n}.(k \nabla T) = h_c(T_s - T_{air}) \tag{7}$$

where **n** is the normal vector to the surface of slab, T_s and T_{air} are surface and ambient temperatures and h_c ($W/m^2.K$) is heat transfer coefficient.

Assuming that provided input power is converted to thermal energy and neglecting heat losses electrical power energy provided to increase slab temperature is calculated as follow,

$$\dot{Q} = P = V.I \tag{8}$$

In Abaqus/Standard, two types of analyses can be performed [58],

1. Coupled thermal-electrical analysis: Electrical potential and temperature fields are solved simultaneously by performing a combined thermal-electrical analysis. In this method, the energy consumed by an electric current flowing through a conductor is converted into thermal energy. In this analysis the deformation of the structure is not taken into account.
2. Piezoelectric analysis: In the piezoelectric material, the electric potential gradient causes stress and stress causes the electric potential in the material. This coupling is achieved by defining the piezoelectric and dielectric coefficients of a material and can be used in natural frequency extraction, transient dynamic analysis, both linear and nonlinear static stress analysis, as well as steady state analysis procedures.

In this study, coupled thermal-electrical analysis, which is a method provided in Abaqus program was used to solve the model.

In electrically conductive concrete required electrical current, is provided by applying the electrical potential to the electrodes embedded in the coating. Electric field in a three-dimensional solid material can be written as [59],

$$E = -\nabla V \tag{9}$$

Here, E is the electric field, V is the electrical potential, and ∇ is the gradient operator.

Heat energy can be calculated in the conductive material as provided in Eq. (7), which indicates thermal energy obtained from electric energy,

$$Q = \boldsymbol{J}.\boldsymbol{E} \text{ and } \boldsymbol{J} = \sigma.\boldsymbol{E} \tag{10}$$

Were σ is the electric conductivity (S mm^{-1}) and $\boldsymbol{J}$ (Amm^{-2}) is current density.

Electrical Analysis Procedures:

The electric field in a conductive material is governed by Maxwell's charge equation. Assuming steady state direct current, the equation can be expressed as,

$$\int_S J.ndS = \int_V r_c dV \tag{11}$$

V is any control volume with a surface S and n is the outward norm number for S. The divergence theorem is used to convert the surface integral to a volume integral,

$$\int_V \left[\frac{\partial}{\partial x}.J - r_c\right] dV = 0 \tag{12}$$

Considering electrical potential field, and integrating over the volume:

$$\int_V \delta\varphi \left[\frac{\partial}{\partial x}.J - r_c\right] dV = 0 \tag{13}$$

Using first the chain rule and then the divergence theorem, this equation is given as,

$$-\int_V \frac{\partial \delta\varphi}{\partial X}.JdV = \int_V \delta\varphi JdS + \int_V \delta\varphi\, r_c dV \tag{14}$$

Assuming that the electrical conductivity is independent of the electrical field and introducing Ohm's law, the obtained governing conservation of the charge equation is written,

$$\int_V \frac{\partial \delta\varphi}{\partial X}.\sigma.\frac{\partial \varphi}{\partial X} dV = \int_S \delta\varphi JdS + \int_V \delta\varphi\, r_c dV \tag{15}$$

Using conservation of the electrical charge and energy balance problem can be explained to solve in the next step. The match consists of two sources: conductivity in electrical problem depends on temperature, $\sigma = \sigma(T)$, and the heat generation in the material is a function of electrical current, $Q = Q(J)$, as described below. Because of the electric current, thermal energy is generated.

Joule's law defines the rate of electrical power emitted by the current flowing through a conductor as $P = E.J$ which can be written in other form as $P = E.\sigma.E$.

Assuming a steady-state condition power (P) can be evaluated at time t + Δt and in a transient analysis an averaged value of P is obtained as follows,

$$P = \frac{1}{\Delta t}\int_{\Delta t} Pdt = E.\sigma.E - E.\sigma.\Delta E + \frac{1}{3}\Delta E.\sigma.\Delta E, \tag{16}$$

where E and σ are values at the time t + Δt

2.5. Finite elements method (FE)

The main objective of this section is to develop a 3D modeling simulation by FE method for evaluating time-based heating performance and optimization in EHPSs. Electrically conductive concrete was simulated in ABAQUS program for elektrothermal analysis and compared to experimental results. EHPS works by applying voltage from the electrodes embedded in a conductive concrete coating.

2.5.1. Simulation process

Coupled thermal-electrical analysis was performed using Abaqus 6.1 as an FE modeling program. The electrical conductivity values of the ECON slabs were defined in the first stage of the study according to the values obtained from the cylindrical specimens (10 cm diameter and 20 height) previously produced in the laboratory. All slab specimens were experimentally tested at first to produce heat at different voltages at the temperature of −10 °C. During the experiments, electrical current values of these specimens at different voltages and different temperatures were also recorded. For use in simulation studies, the thermal conductivity of specimens was measured by ASTM D5334-14 test method [60] and listed in Table 4. In this method, there was no sample size limitation, in the present study, 10 × 10 × 3 cm plate samples were tested. Using the measured current values, conductivity amounts were obtained at each stage. Electrothermal analysis was carried out using these values for each specimen and the results were compared with the experimental results.

2.5.2. Geometry of the model

The ECON slab dimensions were designed as 45 × 45 × 5 cm according to the dimensions of the refrigerator available in the laboratory. Electrode slab is designed as 1 mm thick 45 × 5 cm stainless galvanized steel sheet. In the produced slab specimens, 3 mm diameter screws of 5 cm depth were applied at every 6 cm intervals to ensure adhesion between the electrodes and concrete. In 3D simulation, all details were designed in the same way as shown in Fig. 4. This figure shows the slab dimensions designed in the models and the connection between concrete and electrodes. This method was carried out because the slab specimens were small in size, and it was found that there was a good connection during the experiment. If the samples are large, it is recommended that the electrodes are embedded, as shown in study by Abdualla's [1]. In all models, the initial temperatures of ECON slabs are defined as −10 °C to the mass of the slabs. This temperature limit was selected according to the coldest (−10 °C) temperature of the refrigerator used in the experimental part of the study. Different voltages were applied between the electrodes parallel to the sides of the slabs as the electrical charge in the simulation (Fig. 4b). The applied voltages vary due to the resistance values of the specimen.

2.5.3. Mesh generation

After defining required variables including geometry properties, boundary conditions and material properties, element type and mesh generation was performed. The standard cube element type is used to separate the ECON slab into small elements, as well as the free element type for the electrodes. Different mesh size and number was tested and compared to experimental results and mesh element number of 10,000 was selected to solve the problem. The 3-D mesh view of the ECON slab is given in Fig. 5.

3. Results and discussion

3.1. Basic test results

The authors examined the electrical, mechanical and impact properties of specimens produced from 36 different mixtures in their previous work [34]. According to the results of the experiments, both compressive and flexural strengths of specimens containing NCB, CF, SF and WWE increased. CF has already been successfully used for fabricating ECON for airfield pavement anti-icing and de-icing [18,61–63]. This feature was further enhanced when CF and WWE are used together. Also, by adding NCB (obtained by pyrolysis method from waste tires) in all ECON mixtures, the resistivity values decreased by 2–7 times, and this is the original aspect of the study.

CF, SF and WWE also showed positive effects in increasing the amount of final energy absorbed against impact among the conductive concrete specimens.

Table 4
Basic test results of slab specimen, N: Nano carbon black, C: Carbon fiber, S: Steel fiber, E: Waste wire erosion.

No	Specimen code	Bulk method (Ω.cm)		WPM (Ω.cm)	ASTM-D (Ω.cm)	σ_c (MPa)	σ_f (MPa)	Eu (J)	thermal conductivity (W/m·K)
		Cylinder	slab						
		28 days	28 days	28 days					
1	N10C0.2S0	4915.81	42553	24185.80	7291.02	51.04	7.75	79.31	2.31
2	N6C0.5S0	222.45	4444	560.58	708.27	45.49	7.63	72.84	2.50
3	N6C1S0	80.08	357	188.34	450.72	47.82	8.62	55.03	2.15
4	N10C0.2S2	3979.82	11710	16237.66	5902.26	54.54	6.26	142.44	2.35
5	N6C0.5S2	696.18	7693	2673.34	1652.63	56.99	8.12	200.71	2.48
6	N6C1S2	85.22	371	194.30	413.85	62.01	8.68	234.70	2.44
7	N6 C0E0.5	702.40	5000	1676.55	6352.45	52.24	7.09	192.62	2.44
8	N6 C0E1.0	645.34	2890	1546.33	5720.20	57.87	7.68	236.32	2.88
9	N6C0.2E1.0	254.63	552	376.53	1097.12	41.82	7.58	265.46	2.50
10	N6C0.2E1.5	97.74	270	129.48	441.18	39.52	7.21	254.13	3.09

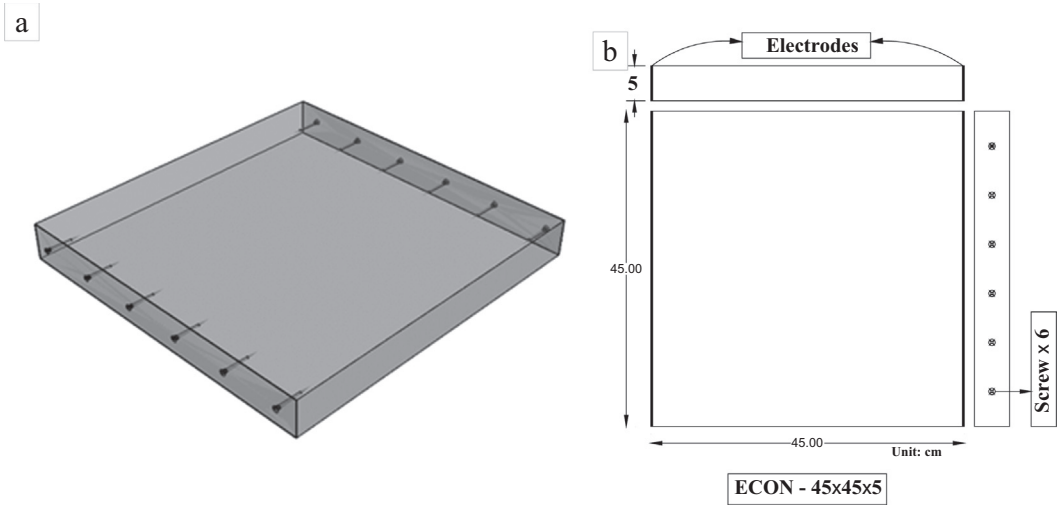

Fig. 4. The 3D view of ECON slab (a) and geometry details of simulated ECON slab (b).

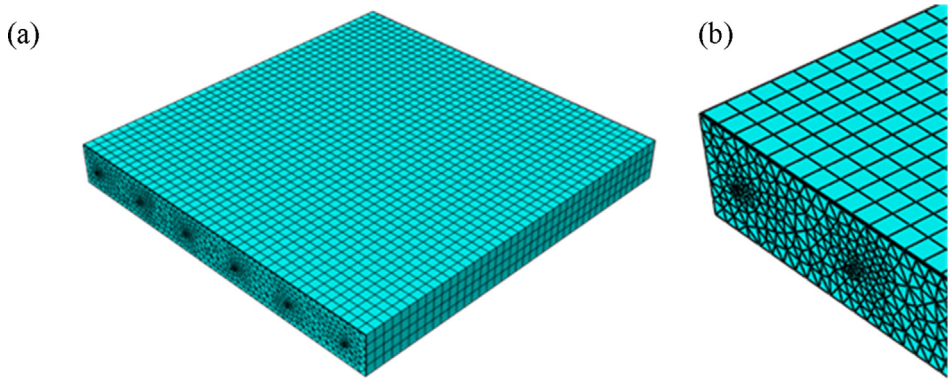

Fig. 5. Mesh generation of ECON slabs (a), magnified electrode and mesh quality around (b).

Electrical measurements were performed on cylindrical and slab specimens of 28 days. The same cylinder specimens used in the electrical test method were then used to determine the 28 day compressive strengths. Flexural test results were obtained from 28-day prismatic specimens. 10 × 10 × 3 cm slab specimens were used to obtain impact energy. The basic test results of 10 ECON slab specimens are given in Table 4.

3.2. Electrothermal results

Time-dependent temperature values of ECON slabs have been measured. Heat and power consumption of the slabs were compared by applying different voltages in both simulation and experimental methods. No rules are used to select voltage values. The test times were chosen depending on the temperature of the specimens. For rapid-warming specimens, the experiment was terminated prematurely and for slow-warming specimens, it was terminated late. For all mixtures, the measured resistivity values in the cylinder specimens were lower than the resistivity values of the slab specimens, which provided misleading information in 3D electrothermal results. This problem is also mentioned in previous research [1]. Therefore, in this study, firstly, 3D modeling was performed according to the conductivity properties of the cylinder specimens. In order to verify the thermal results of the slabs pro-

duced in the next step, 3D modeling was done according to the conductivity properties of the slab specimens.

Electrothermal results of the slab specimen of the mixture containing 6 wt% NCB and 0.2 vol% CF are obtained at different voltages given in Table 5. Since the measured electrical resistivity values of this mixture were high, no significant temperature increase was observed at different voltages applied in both the 3D simulation and experimental results. Test results have been recorded during 480 min by applying various voltages in experiments. The resistivity values measured for this mixture at room temperature were 4916 and 42553 Ω.cm for cylinder and slab specimens, respectively.

The resistivity values of the cylinder specimens of the mixture containing 6 wt% NCB and 0.5 vol% CF were also lower than the resistivity values of the slab specimens. In other words, the cylindrical electrical conductivity of the specimens was recorded more than the plate-shaped specimens. The resistivity values measured for this mixture at room temperature were 223 and 4444 Ω.cm for the cylinder and slab specimens, respectively. For this specimen, the higher the potential difference applied, the higher the temperature values were recorded. With the voltage of 140 V, the temperature has increased from −10 °C to 0 °C. When the voltage rises to 180 V, the temperature increases from −10 °C to 10 °C. The temperature rises above 25 °C when the applied voltage value is 220 V. Obtained results in the table show the similarities between experimental and modeling results of the electrothermal behavior applying four different voltages. In the modeling and experimental results, by applying 220 V voltage, the temperature increase rate decreased after a certain time. The reason is that, after applying voltage to the slab specimen, the rate of the electrical current increases with the initial increase in temperature, and then the rate of increase of the current decreases after the temperature reaches a certain degree. Conductivity values were calculated according to the current values measured at different temperatures during the experiment and the same values were used in the Abaqus program. Electrothermal results of the slab specimen containing 6 wt% NCB and 1 vol% CF are also given in the table. Since the resistivity values of the specimens of this mixture were lower than the other mixtures, the electrothermal results were also more favorable than the other mixtures. Resistivity values of slab specimens at room temperature were measured as 357 Ω.cm. In addition, in all voltage applications, obtained results show that, the temperature increase rate is low in the first time intervals (0–30 min) and increases after a certain time. The reason for this is that, the electrical current is low at first when the temperature of the concrete is at low levels (-10 °C) and increases gradually over the test time. The applied 60, 80, 100 and 120 V voltage values have generated sufficient heat power to melt the ice. As a result of applying 60 V, the temperature increased by approximately 16°-within 4 h. The results for the other voltage values are also presented. Furthermore, there is a good agreement between the model and experimental results. The resistivity measured for the N6C0.2S2 mixture was 11710 Ω.cm in the plate specimens. No significant electrothermal results were obtained as the resistivity value was high. Similar results were also recorded for the steel fiber-free mixture of the same mixture (See Section 3.2.1). From the experiment of N6C0.5S2, it was found that the use of 2 wt% SF has a negative effect on heat energy. This may be due to the reduced conductivity due to the heterogeneity of the mixture due to reduced workability with the combined use of CF and SF.

According to the results of the voltage applied to the plate specimen N6C1S2, it was observed that, voltages above 80 V are approprite for heastnig specimens. However, this mixture is not recommended as there is no significant difference in heat energy compared to the N6C1S0 mixture. From the results of electrical resistance, WWE has been shown important role in electrothermal experiments since it has good electrical conductivity. Resistance values of plate specimens having N6C0E0.5 mixture were measured as 7500 Ω.cm. Resistance values decreased with increasing WWE content and adding 0.2 vol% CF to the mixtures. Obtained results by applying 100, 140, 180 and 220 V have been presented in Table 5. According to the results of the N6C0E1 specimen, by applying voltages between 100 and 220 V. An increase of 20 °C was recorded after 480 min by 140 V. When 180 and 220 V were applied, 300 and 200 min time were required to achieve the same temperature. The effect of the addition of 0.2 CF to the N6C0E1 mixture on the electrothermal properties is provided in Table 5. After applying 60, 80, 100 and 120 V, to the N6C0.2E1 plate specimen, it took 480, 240, 180 and 120 min, respectively, for increasing temperature from −10 °C, to about +10 °C. Since N6C0.2E1 and N6C0.2E1.5 specimens had low electrical conductivity among WWE-containing plate specimens, both were found to have sufficient heat generation potential at low voltages and durations according to the electrothermal test results. However, during mixing, N6C0.2E1.5 had problems in mixing and placing due to the low workability of the mixture.

The comparison of ten different mixtures was considered and obtained results in different voltages was presented and discussed. However, in this section the constant voltage of 100 V is considered to have a comparison between all test specimens. Therefore, Fig. 6 are given to compare specimen results in the same voltage. As explained in the sections above, 100 V is a high voltage for the specimens N6C0.2E1.5, N6C1S0 and N6C1S2, and 80 V has been proposed for these specimens to be heated more properly. For the specimen N6C0.2E1 100 V is considered appropriate for heating up to 10 °C within 180 min. It has been seen that, the specimens N10C0.2S0 and N10C0.2S2 cannot be heated in this situation and they have shown behavior as insulation materials.

3.3. Average power consumed values

The amount of average electrical power (P) consumed by applying 60, 80, 100, 120, 180 and 220 V voltage for under test specimens was calculated respectively (Fig. 7). In the N6C0.5S0, the increase of 1.5 times of the power is due to the increase of the current amount in the applied voltage. From the literature [1,64,65], it has been stated that 300–550 W/m^2 power is required for melting snow and ice in cold weather. Therefore, within a short period of time, the melting potential is not expected from this specimen. For the power calculation, current and voltage values were used as previously explained in the section equation.

For the N6C1S0 specimen, the electrical power consumed at each voltage above 60 V was found to be sufficient for defrosting. It was also determined that the minimum of 425 W/m^2 heat power has been consumed for heating the N6C1S2 slab specimen at 80 V. With the increase of the voltage value to 100 and 120 V, the power consumption consumed increased by 0.56 and 1.25 times respectively. Compared to N6C1S0, this slab contains 2 wt% SF, but there is no significant difference in the power consumed for heating. Therefore, this mixture is not recommended for application. For the N6C0.2E1 specimen containing 1 wt% WWE, the obtained power values are considered to be suitable for the heating of the concrete specimens in a short time by applying three different voltages as shown in the figure.

As a result of 80 V and power consumption of 286 W/m^2, heating application is not appropriate but, 447 W/m^2 power consumption as a result of 100 V application, is considered suitable both in terms of heating time and energy consumption. In order to prevent snow and ice accumulation, 516 W/m^2 in the study by Yehia and Tuan [66] and also 300–350 W/m^2 in the study by Sassani et al. [67] have been proved to be sufficient. The heating rate of 643 W/m^2 cause to fast warming, but leads to increased energy

Table 5
Electrothermal test results of slab specimen, N: Nano carbon black, C: Carbon fiber, S: Steel fiber, E: Waste wire erosion.

Specimen code	voltage	Time (min)	0	30	60	90	120	150	180	210	240	270	300	330	360	390	420	450	480
N10C0.2S0	100 V	Exp	−10.0	−10.0	−10.0	−10.0	−10.0	−10.0	−10.0	−9.9	−9.9	−9.9	−9.9	−9.9	−9.9	−9.9	−9.9	−9.9	−9.9
		Model	−10.0	−10.0	−10.0	−10.0	−9.9	−9.9	−9.9	−9.9	−9.9	−9.9	−9.8	−9.8	−9.8	−9.8	−9.8	−9.8	−9.7
	140 V	Exp	−10.0	−10.0	−10.0	−10.0	−10.0	−10.0	−10.0	−9.9	−9.9	−9.9	−9.8	−9.8	−9.8	−9.7	−9.7	−9.7	−9.6
		Model	−10.0	−10.0	−10.0	−9.9	−9.9	−9.9	−9.8	−9.8	−9.8	−9.7	−9.7	−9.7	−9.6	−9.6	−9.6	−9.5	−9.5
	180 V	Exp	−10.0	−10.0	−10.0	−10.0	−10.0	−10.0	−9.9	−9.8	−9.8	−9.7	−9.7	−9.6	−9.6	−9.5	−9.4	−9.4	−9.3
		Model	−10.0	−10.0	−9.9	−9.9	−9.8	−9.8	−9.7	−9.7	−9.6	−9.5	−9.5	−9.4	−9.4	−9.3	−9.2	−9.2	−9.1
	220 V	Exp	−10.0	−10.0	−10.0	−9.9	−9.8	−9.8	−9.7	−9.6	−9.5	−9.4	−9.4	−9.3	−9.2	−9.0	−8.9	−8.8	−8.7
		Model	−10.0	−10.0	−9.9	−9.8	−9.7	−9.6	−9.6	−9.5	−9.4	−9.3	−9.2	−9.1	−9.0	−8.9	−8.8	−8.7	−8.6
N6C0.5S0	100 V	Exp	−10.0	−9.9	−9.9	−9.8	−9.8	−9.7	−9.7	−9.7	−9.5	−9.2	−9.0	−8.7	−8.5	−8.2	−8.0	−7.9	−7.8
		Model	−10.0	−9.9	−9.7	−9.5	−9.3	−9.1	−8.9	−8.7	−8.5	−8.2	−8.0	−7.7	−7.5	−7.2	−6.9	−6.6	−6.3
	140 V	Exp	−10.0	−10.0	−9.9	−9.8	−9.5	−9.1	−8.6	−7.7	−7.1	−6.8	−6.1	−5.4	−4.6	−3.7	−3.0	−2.5	−1.6
		Model	−10.0	−9.8	−9.4	−9.0	−8.5	−8.1	−7.6	−7.0	−6.4	−5.8	−5.1	−4.4	−3.6	−2.7	−1.8	−0.7	0.3
	180 V	Exp	−10.0	−9.5	−9.9	−9.2	−8.7	−8.3	−7.2	−6.0	−4.5	−2.9	−0.8	2.1	3.6	5.1	6.8	7.6	9.0
		Model	−10.0	−9.6	−8.9	−8.2	−7.3	−6.3	−5.2	−4.0	−2.5	−0.9	0.9	2.8	4.8	6.8	9.0	11.2	13.6
	220 V	Exp	−10.0	−9.5	−9.0	−7.3	−5.3	−3.2	−1.2	0.9	2.9	4.5	6.4	10.0	15.6	19.0	21.5	24.9	25.5
		Model	−10.0	−9.4	−8.3	−7.0	−5.3	−3.4	−1.0	1.7	4.7	7.8	11.1	14.8	18.8	23.1	27.2	29.9	31.8
N6C1S0	60 V	Exp	−10.0	−9.0	−6.8	−5.0	−3.3	−1.2	1.0	2.8	6.4	–	–	–	–	–	–	–	–
		Model	−10.0	−8.9	−7.0	−5.0	−2.8	−0.3	2.5	5.6	9.0	–	–	–	–	–	–	–	–
	80 V	Exp	−10.0	−8.8	−6.4	−2.0	3.3	10.0	15.5	24.1	27.1	–	–	–	–	–	–	–	–
		Model	−10.0	−7.9	−4.2	0.2	5.5	11.9	18.9	26.3	32.0	–	–	–	–	–	–	–	–
	100 V	Exp	−10.0	−7.4	−1.0	7.0	18.7	27.2	32.4	37.9	43.3	–	–	–	–	–	–	–	–
		Model	−10.0	−6.5	0.2	9.3	20.3	30.6	37.5	43.9	50.3	–	–	–	–	–	–	–	–
	120 V	Exp	−10.0	−5.2	6.1	20.2	32.0	39.0	47.0	53.0	57.5	–	–	–	–	–	–	–	–
		Model	−10.0	−4.6	7.4	23.6	35.0	44.4	53.6	62.8	72.0	–	–	–	–	–	–	–	–
N10C0.2S2	100 V	Exp	−10.0	−10.0	−9.9	−9.9	−9.8	−9.8	−9.8	−9.7	−9.6	−9.6	−9.5	−9.4	−9.4	−9.3	−9.2	−9.1	−9.1
		Model	−10.0	−10.0	−9.9	−9.8	−9.8	−9.7	−9.7	−9.6	−9.5	−9.5	−9.4	−9.3	−9.3	−9.2	−9.1	−9.1	−9.0
	140 V	Exp	−10.0	−10.0	−9.9	−9.8	−9.8	−9.7	−9.7	−9.6	−9.7	−9.6	−9.5	−9.3	−9.1	−9.0	−8.8	−8.7	−8.7
		Model	−10.0	−9.9	−9.8	−9.7	−9.6	−9.4	−9.3	−9.2	−9.0	−8.9	−8.8	−8.6	−8.4	−8.3	−8.1	−7.9	−7.8
	180 V	Exp	−10.0	−10.0	−9.9	−9.9	−9.8	−9.7	−9.5	−9.3	−9.0	−8.7	−8.2	−7.7	−7.5	−7.2	−7.1	−6.1	−5.7
		Model	−10.0	−10.0	−9.9	−9.7	−9.6	−9.5	−9.1	−8.8	−8.4	−8.0	−7.6	−7.3	−6.9	−6.5	−6.1	−5.8	−5.4
	220 V	Exp	−10.0	−9.5	−9.8	−9.5	−9.7	−9.3	−8.9	−8.5	−8.0	−7.5	−6.9	−6.3	−5.6	−4.9	−4.1	−3.2	−2.9
		Model	−10.0	−9.8	−9.5	−9.2	−8.8	−8.4	−8.0	−7.6	−7.1	−6.6	−6.0	−5.4	−4.7	−4.0	−3.2	−2.3	−1.4
N6C0.5S2	100 V	Exp	−10.0	−10.0	−10.0	−10.0	−10.0	−9.9	−9.7	−9.6	−9.5	−9.4	−9.3	−9.2	−9.1	−9.0	−8.8	−8.7	−8.7
		Model	−10.0	−9.9	−9.9	−9.8	−9.7	−9.6	−9.5	−9.4	−9.3	−9.2	−9.1	−9.0	−8.8	−8.7	−8.6	−8.5	−8.4
	140 V	Exp	−10.0	−10.0	−9.9	−9.8	−9.8	−9.5	−9.4	−9.3	−9.1	−8.9	−8.5	−8.3	−8.1	−7.8	−7.4	−7.3	−7.2
		Model	−10.0	−9.9	−9.7	−9.5	−9.3	−9.1	−8.9	−8.7	−8.4	−8.2	−7.9	−7.6	−7.4	−7.1	−6.7	−6.4	−6.0
	180 V	Exp	−10.0	−10.0	−9.8	−9.6	−9.4	−9.0	−8.5	−8.1	−7.6	−7.3	−6.5	−5.8	−5.1	−4.4	−3.7	−2.9	−2.4
		Model	−10.0	−9.8	−9.5	−9.2	−8.8	−8.4	−8.0	−7.5	−7.0	−6.5	−5.9	−5.2	−4.5	−3.8	−3.0	−2.1	−1.1
	220 V	Exp	−10.0	−9.9	−9.8	−9.6	−8.9	−8.2	−7.8	−6.5	−5.5	−4.3	−3.5	−2.0	0.1	1.9	3.7	5.5	6.5
		Model	−10.0	−9.7	−9.2	−8.7	−8.0	−7.3	−6.5	−5.6	−4.6	−3.4	−2.1	−0.6	1.0	2.8	4.6	6.6	8.8
N6C1S2	60 V	Exp	−10.0	−9.8	−9.6	−8.5	−7.4	−5.9	−4.2	−2.9	−0.1	2.7	4.8	–	–	–	–	–	–
		Model	−10.0	−9.8	−9.0	−8.0	−6.9	−5.4	−3.7	−1.6	0.9	3.7	6.8	–	–	–	–	–	–
	80 V	Exp	−10.0	−9.2	−8.0	−6.5	−3.5	1.5	7.8	13.2	19.0	–	–	–	–	–	–	–	–
		Model	−10.0	−9.1	−7.4	−4.9	−1.3	3.3	9.1	15.6	22.7	–	–	–	–	–	–	–	–
	100 V	Exp	−10.0	−8.5	−5.9	0.1	7.7	17.6	26.5	32.0	34.0	–	–	–	–	–	–	–	–
		Model	−10.0	−8.5	−4.7	1.8	11.0	21.9	30.8	35.3	38.8	–	–	–	–	–	–	–	–
	120 V	Exp	−10.0	−5.2	4.3	14.1	24.1	31.1	36.2	38.1	40.6	–	–	–	–	–	–	–	–
		Model	−10.0	−7.4	1.0	14.8	29.2	35.8	40.7	45.6	50.5	–	–	–	–	–	–	–	–
N6C0E0.5	100 V	Exp	−10.0	−10.0	−9.9	−9.9	−9.8	−9.7	−9.6	−9.4	−9.2	−8.9	−8.8	−8.5	−8.3	−8.1	−8.1	−8.0	−7.8
		Model	−10.0	−9.9	−9.8	−9.7	−9.5	−9.4	−9.2	−9.1	−8.9	−8.7	−8.6	−8.4	−8.2	−8.0	−7.8	−7.6	−7.4
	140 V	Exp	−10.0	−9.9	−9.7	−9.6	−9.2	−8.9	−8.2	−7.4	−7.0	−6.7	−6.0	−5.4	−4.7	−3.8	−3.6	−3.3	−3.0
		Model	−10.0	−9.8	−9.6	−9.3	−9.0	−8.7	−8.3	−7.9	−7.5	−7.1	−6.6	−6.1	−5.6	−5.0	−4.4	−3.7	−3.0
	180 V	Exp	−10.0	−9.7	−9.2	−8.5	−7.8	−6.0	−5.3	−3.8	−3.0	−1.9	−1.0	0.8	1.0	2.0	3.0	4.0	5.4
		Model	−10.0	−9.7	−9.3	−8.7	−8.1	−7.5	−6.7	−5.9	−4.9	−3.8	−2.6	−1.2	0.3	2.0	3.7	5.6	7.7
	220 V	Exp	−10.0	−9.5	−9.1	−8.2	−6.0	−4.2	−2.9	−0.3	1.8	4.4	7.8	9.0	11.8	13.7	17.6	22.0	25.1
		Model	−10.0	−9.6	−8.8	−7.9	−6.8	−5.5	−3.9	−2.0	0.3	2.8	5.6	8.7	12.0	15.5	19.3	23.2	27.2
N6C0E1	100 V	Exp	−10.0	−10.0	−9.8	−9.7	−9.3	−9.0	−8.4	−8.0	−7.4	−7.1	−6.6	−6.0	−5.7	−5.4	−5.0	−4.7	−4.0
		Model	−10.0	−9.9	−9.5	−9.2	−8.8	−8.4	−8.0	−7.5	−7.1	−6.6	−6.1	−5.6	−5.0	−4.5	−3.9	−3.2	−2.6
	140 V	Exp	−10.0	−9.8	−9.3	−8.7	−8.0	−7.4	−6.5	−5.3	−4.4	−3.2	−2.3	0.0	1.1	2.5	3.7	5.9	8.1
		Model	−10.0	−9.8	−9.0	−8.2	−7.4	−6.4	−5.4	−4.2	−3.0	−1.6	−0.1	1.4	3.0	4.6	6.2	7.8	9.5
	180 V	Exp	−10.0	−9.7	−9.4	−8.8	−7.9	−5.8	−3.9	−1.2	1.9	3.8	8.9	13.7	18.3	22.3	26.9	31.1	34.2
		Model	−10.0	−9.6	−8.3	−6.8	−5.0	−2.9	−0.5	2.0	4.7	7.4	10.2	13.5	17.2	21.5	25.9	28.7	30.6
	220 V	Exp	−10.0	−9.0	−6.9	−4.8	−1.9	2.4	6.0	13.4	15.4	19.0	22.5	26.0	28.5	32.2	35.9	39.4	41.1
		Model	−10.0	−8.8	−6.6	−3.8	−0.4	3.4	7.5	11.8	17.1	21.5	26.0	29.8	33.6	36.4	39.1	41.5	43.5
N6C0.2E1	60 V	Exp	−10.0	−9.9	−9.8	−9.7	−9.2	−8.1	−6.8	−6.2	−5.4	−4.3	−3.1	−1.7	−0.1	2.0	4.2	6.1	8.0
		Model	−10.0	−9.9	−9.4	−8.8	−8.1	−7.4	−6.6	−5.6	−4.5	−3.3	−1.8	−0.2	1.6	3.4	5.5	7.6	9.9
	80 V	Exp	−10.0	−9.7	−9.0	−8.1	−6.9	−5.0	−1.8	0.5	7.6	12.1	17.2	21.2	23.9	25.8	28.9	31.6	33.9
		Model	−10.0	−9.7	−8.7	−7.4	−5.7	−3.5	−0.8	2.5	6.1	10.2	14.6	19.2	24.1	27.9	30.6	32.8	34.6
	100 V	Exp	−10.0	−9.0	−8.0	−4.4	−0.5	3.3	8.5	14.2	21.2	–	–	–	–	–	–	–	–
		Model	−10.0	−9.1	−7.1	−4.2	0.0	5.4	11.7	18.7	26.0	–	–	–	–	–	–	–	–

Table 5 (*continued*)

Specimen code	voltage	Time (min)	0	30	60	90	120	150	180	210	240	270	300	330	360	390	420	450	480
	120 V	Exp	−10.0	−9.0	−3.7	3.8	12.7	23.0	27.9	30.6	33.4	–	–	–	–	–	–	–	–
		Model	−10.0	−8.5	−4.7	1.6	10.3	20.6	29.4	34.4	38.1	–	–	–	–	–	–	–	–
N6C0.2E1.5	60 V	Exp	−10.0	−9.7	−8.8	−7.9	−5.4	−0.6	2.6	7.2	12.0	–	–	–	–	–	–	–	–
		Model	−10.0	−9.7	−8.3	−6.4	−3.9	−0.6	3.5	8.1	13.2	–	–	–	–	–	–	–	–
	80 V	Exp	−10.0	−8.0	−4.2	−1.5	5.7	15.3	–	–	–	–	–	–	–	–	–	–	–
		Model	−10.0	−8.5	−5.1	0.7	8.6	17.8	–	–	–	–	–	–	–	–	–	–	–
	100 V	Exp	−10.0	−6.0	2.9	13.6	22.4	–	–	–	–	–	–	–	–	–	–	–	–
		Model	−10.0	−7.2	1.6	15.2	28.5	–	–	–	–	–	–	–	–	–	–	–	–
	120 V	Exp	−10.0	−3.0	10.4	27.5	35.8	–	–	–	–	–	–	–	–	–	–	–	–
		Model	−10.0	−4.6	13.7	30.8	37.3	–	–	–	–	–	–	–	–	–	–	–	–

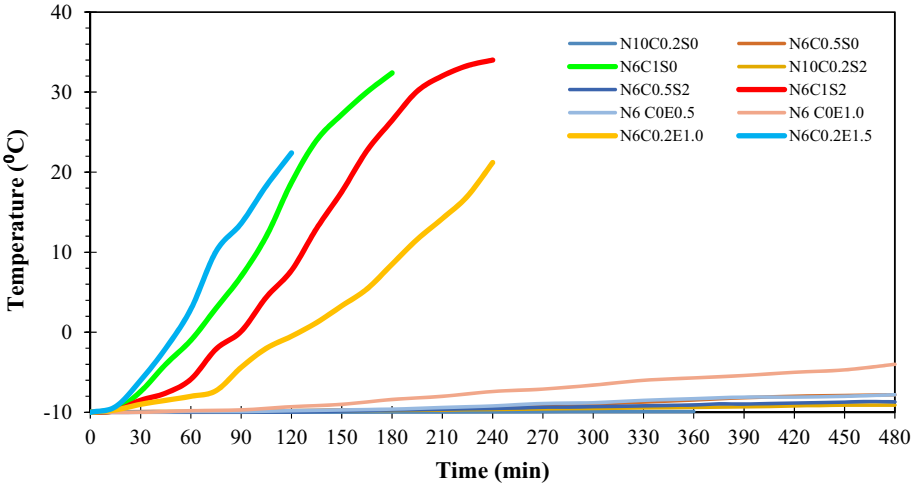

Fig. 6. Electrothermal results at 100 V for all slab specimens.

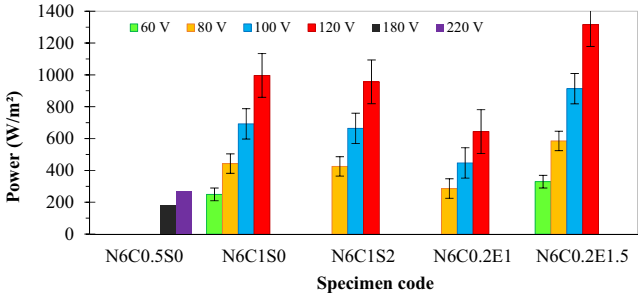

Fig. 7. Average consumed power in different applied voltages for different specimens.

losses, leading to increased operating costs. In the case of N6C0.2E1.5, all the voltages applied above 60 V have sufficient heat power values to warm up in the desired time. Since the appropriate power values are determined as 300–550 W/m^2 in the literature, minimum of 329 W/ m^2 has been recorded as a result of 60 V, which is appropriate for this specimen. If it is desired to increase the heating rate, the result of 589 W/m^2 by applying 80 V can be considered.

3.4. Temperature distribution obtained by simulation

According to the results of the specimens and literature studies, N6C1S0 and N6C0.2E1.5 mixtures are considered to be suitable for ice solution in low time intervals compared to other mixtures. Thus, for these specimens only, the temperature distribution of these specimens are given when applied voltage is 60 and 80 V.

Temperature contours obtained according to experimental results and FE modeling results are given in Fig. 8. Experimental images were plotted using SURFER 9 program by applying temperature results obtained from 9 different points at slab specimens. Temperature distribution of specimen N6C0.2E1.5 has been obtained by applying 80 V during 150 min, FE results and experimental results have been provided in Fig. 8- a and b. highest temperature values have been recorded in this condition and most part of specimen colored by red which indicated higher temperature values. In addition, for the same specimen (N6C0.2E1.5) voltage of 60 V has been also applied during 240 min and results are obtained as illustrated in Fig. 8-c and d. In addition, Fig. 8-e and f has been presented to show results of the specimen N6C1S0 at voltage value of 80 V over the test time of 240 min. Furthermore, FE and experimental results of specimen N6C1S0 at 60 V and 240 min are given in Fig. 8-g and h. The temperature difference of approximately 1 °C on the bottom and top of the specimen, may be occurred due to the high CF dosage, resulting a non-uniform distribution of the CF. The compatibility between the experimental and FE modeling results for this specimen can also be seen in the figure. In the Abaqus program conductive concrete is defined as homogeneous. As a result, due to the assumption of homogeneous concrete in FE simulation, the temperature range on the slab surface was narrow. However, the mean temperature values of the slab specimens are very close to each other in the FE and experimental method.

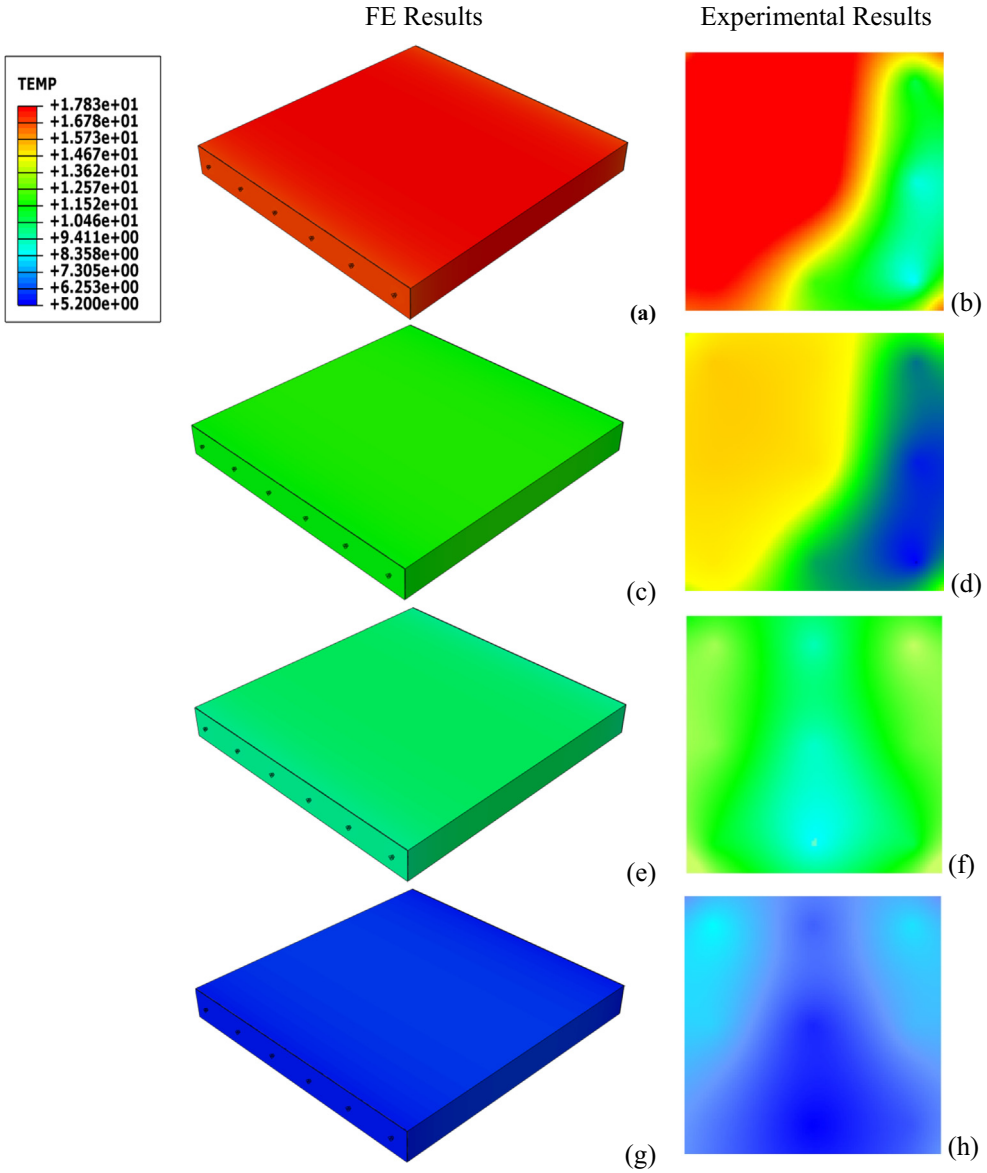

Fig. 8. Temperature distribution in test specimens (a & b); N6C0.2E1.5 – 80 V, (c & d); N6C0.2E1.5 – 60 V, (e & f); N6C1S0 – 80 V, (g & h); N6C1S0 – 60 V.

3.5. Performance evaluation in ECONs

The performance of 6 ECON slabs selected from ten different specimens is given in Table 6. The specimens in this table are those with heating capacities from −10 °C to +10 °C under 6 h as a result of the different voltages applied. For example, as a result of applying 220 V to N6C0.5S0, power of 268.89 W/m^2 was consumed during 5.5 h and an increase of 20 °C was observed in the temperature.

For specimen N6C1S0, 442.9 W/m^2 of power was sufficient to increase the temperature to 10 °C by applying 80 V for 2.5 h. However, the production cost of this specimen increased by 84% compared to the previous specimen, while the capital cost decreased by 25%. Mentioned specimens have been compared in details in the term of voltage, time, power, energy production cost and energy cost as provided in the table.

3.6. Mixture optimization and specimen Selection

In this part of the study, it is aimed to select the most suitable specimen by considering different criteria according to all the results obtained as described in follows,

In the case of production cost, which includes all materials and labor costs, since it is a one-time use material type, ECONs with different materials may have a low coefficient of production cost compared to the operating cost. During the optimization, the production cost coefficient was accepted as 5%. For the operational cost of the ECON (includes the cost of consumed electrical energy) the coefficient of this criterion is taken into account as 10% in the optimization process. The most important factor affecting performance is the resistivity of concrete. According to the results, the specimens with the lowest resistivity showed the best performance. The coefficient of the resistivity factor was 35%.

According to the findings of this study, since the compressive strength of all specimens is tested above 40 MPa, the effect of this factor is less considered and was calculated as 10%. Another factor is heating time. Generally, the purpose of the application of ECONs is to heat up the concrete in a short time and so as an important factor, its coefficient is accepted as 25%. In the case of workability of concrete, the requirements related to workability of concrete during mixing can affect both the strength of the concrete and the resistance. The coefficient of this factor is taken into account as 10%. Finally, the coefficient of factors Nativity (Locality) and

Table 6
Time and energy required to increase the temperature from −10° C to +10° C.

NO	Specimen code	Voltage (V)	Time (h)	Power (W/m^2)	Energy (kW.h/m^2)	Production cost ($/m^2)	Energy cost ($/m^2)
1	N6C0.5S0	220	5.5	268.89	1.48	26.80	0.220
2	N6C1S0	80	2.5	442.9	1.11	49.16	0.163
3	N6C1S2	80	3.2	425.09	1.36	52.08	0.200
4	N6C0E1	220	3.4	406.48	1.38	15.42	0.204
5	N6C0.2E1	100	4	446.9	1.79	136.50	0.263
6	N6C0.2E1.5	80	2.2	584.74	1.29	29.88	0.189

Note: The values are calculated for a 5 cm thick concrete slab.

Table 7
Raw values used for optimization.

No	Specimen code	Production cost ($/m2)	Operating cost ($/m2)	Resistivity (Ω.cm)	Compressive strength (MPa)	Warming time (h)	Workability of concrete	Locality	Continuity
1	N6C0.5S0	26.80	0.220	4444	45.49	5.5	7.5	5	10
2	N6C1S0	49.16	0.163	357	47.82	2.5	5	2.5	10
3	N6C1S2	52.08	0.200	371	62.01	3.2	3	2.5	10
4	N6C0E1	15.42	0.204	2890	57.87	3.4	6	10	5
5	N6C0.2E1	136.50	0.263	552	41.82	4	6	8	5
6	N6C0.2E1.5	29.88	0.189	270	39.52	2.2	4	8	3.5

Table 8
Selection of specimens according to different criteria.

No	Specimen code	Production cost	Operating cost	Resistivity	Compressive strength	Warming time	Workability of concrete	Locality	Continuity	Efficiency value
1	N6C0.5S0	−0.05	−0.10	−0.35	0.10	−0.25	0.75	0.10	0.30	0.50
2	N6C1S0	−0.09	−0.07	−0.03	0.11	−0.11	0.50	0.05	0.30	0.65
3	N6C1S2	−0.10	−0.09	−0.03	0.14	−0.15	0.30	0.05	0.30	0.42
4	N6C0E1	−0.03	−0.09	−0.23	0.13	−0.15	0.60	0.20	0.15	0.57
5	N6C0.2E1	−0.05	−0.12	−0.04	0.09	−0.18	0.60	0.16	0.15	0.61
6	N6C0.2E1.5	−0.06	−0.09	−0.02	0.09	−0.10	0.40	0.16	0.11	0.49

Continuity were calculated as 2% and 3% respectively. Continuity can be explained as the availability of the used materials in the both form of domestic or even foreign imports which is a significant factor during production.

Table 7 gives the raw values used for optimization. The values of production cost, operating cost, resistivity, compressive strength and heating time criteria were taken into account. For the workability criterion of concrete, a value between 2 and 7.5 was determined according to different mixtures. A value of less than 10 was accepted according to the different mixtures for the criterion of locality and continuity. The values of all specimen in table 6, were firstly divided by the values of the first specimen (N6C0.5 s0) and then, final values have been obtained by multiplying all the values by the relevant coefficients as shown in Table 8.

According to the described criteria, optimization analysis was performed for different specimens in Table 8 and an efficiency value was calculated for each specimen. The efficiency value was obtained by adding all criterion values for each specimen.

The minus and plus signs in the table relate to the disadvantage and advantage of the criteria for the specimen, respectively. The maximum efficiency value was determined to belong to N6C1S0 specimen. In Fig. 9, the rankings of the specimens is given for comparing efficiency values.

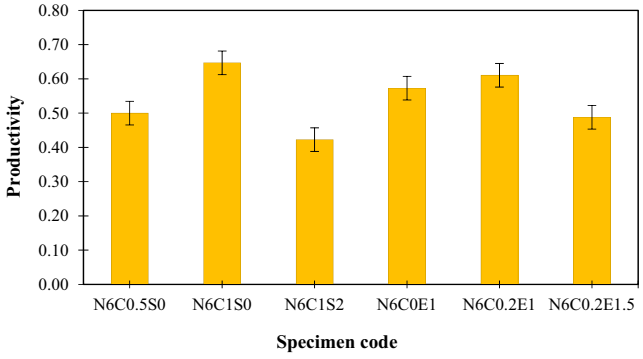

Fig. 9. Calculated efficiency values for different specimens.

4. Conclusion

In this study it was revealed that, the best results were obtained for N6C1S0 and N6C0.2E1.5 specimens in terms of electrical conductivity. Resistance value of N6C1S0 mixture was measured as 80 Ω.cm in cylinder specimens and 357 Ω.cm in slab specimens. For N6C0.2E1.5 mixture, the resistivity values of the cylinder and slab specimens were 98 and 270 Ω.cm, respectively. It was observed that, nano carbon black, carbon fiber and steel fiber materials used in the mixture did not show any negative effect on the compressive strength of concrete. In addition, the compressive strength of most specimens was obtained above 50 MPa, whereas the compressive strength of the normal specimen was measured as 44 MPa. The flexural strength of all produced conductive concretes were increased compared to that of the normal specimen (~5 MPa). By using different amounts of nano carbon black and 2 wt% steel

fiber, the specimen containing 3 wt% nano carbon black showed a higher result (9.02 MPa). The flexural strength of Electrically conductive concrete (ECON) specimens containing waste wire erosion increased by up to 54% compared to the normal specimen. From the impact test, comparing steel fiber and carbon fiber results, the most important factor affecting the impact energy is steel fiber. Under test specimens were analyzed and good agreement between experimental and simulation by Abaqus, was observed. 80 V and 100 V voltage values for N6C1S0, N6C0.2E1.5 and N6C1S2 ECON specimens were found suitable. However, it was determined that 220 V voltage is required for appropriate temperature changes of N6C0.5S0, N6C0E1 specimens. The power consumption of 180–1315 W/m^2 was used to warm the ECON slabs obtained from different mixtures. From the literature, however, at least 300 W/m^2 power is required for melting snow and ice in cold regions. Therefore, in this study, considering the heating time and cost, power values between 300 and 550 W/m^2 are recommended. Different criteria as production cost, operating cost, resistivity, compressive strength, heating performance, workability, locality and continuity have been considered by optimization analysis. According to the optimization results, N6C1S0 specimen was found to be more suitable than other specimens. The most negative aspect of waste wire erosion -containing blends is the agglomeration of the fibers in the blend and the prevention of homogeneity. Also Federal Aviation Administration (FAA) is so adamant that such materials should not be used in the paved areas of airfields, as they can turn into foreign object debris (FOD). By using shorter waste wire erosion, the problem of agglomeration in the mixture can be investigated, and if positive results are obtained, it can be used in non-airport applications.

CRediT authorship contribution statement

Heydar Dehghanpour: Conceptualization, Investigation, Formal analysis, Methodology, Software, Resources, Writing - review & editing. **Kemalettin Yilmaz:** Supervision, Investigation, Validation, Project administration, Writing - review & editing. **Faraz Afshari:** Investigation, Formal analysis, Writing - review & editing. **Metin Ipek:** Supervision, Validation, Methodology.

Declaration of Competing Interest

The authors declare that they have no known competing financial interests or personal relationships that could have appeared to influence the work reported in this paper.

Acknowledgements

Authors wish to thank Sakarya University for technical assistance. Also, authors would like to thank TÜBİTAK for the financial support of this study. (Project number: 119M164).

References

[1] H. Abdualla, Design, Construction, and Performance of Heated Concrete Pavements System. Doctor of Philosophy Thesis. Iowa State University, 2018.
[2] A. Arabzadeh, H. Ceylan, S. Kim, A. Sassani, K. Gopalakrishnan, M. Mina, Electrically-conductive asphalt mastic: Temperature dependence and heating efficiency, Mater. Des. 157 (2018) 303–313.
[3] S. Yehia, C.Y. Tuan, Conductive concrete overlay for bridge deck deicing, Mater. J. 96 (3) (1999) 382–390.
[4] H. Xu, Y. Tan, Development and testing of heat-and mass-coupled model of snow melting for hydronically heated pavement, Transp. Res. Rec. 2282 (1) (2012) 14–21.
[5] A. Arabzadeh, M.A. Notani, A.K. Zadeh, A. Nahvi, A. Sassani, H. Ceylan, Electrically conductive asphalt concrete: An alternative for automating the winter maintenance operations of transportation infrastructure. Compos. Part B: Eng., 2019: 106985.
[6] R. Rao, J. Fu, Y. Chan, C.Y. Tuan, C. Liu, Steel fiber confined graphite concrete for pavement deicing, Compos. Part B Eng. 155 (2018) 187–196.
[7] M. Joerger, F. Martinez, Electrical Heating of I-84 in Land Canyon, Oregon. 2006, Report No. FHWA-OR-RD06-17. Oregon Department of Transportation, Salem, OR.
[8] R. Rao, H. Wang, H. Wang, C.Y. Tuan, M. Ye, Models for estimating the thermal properties of electric heating concrete containing steel fiber and graphite, Compos. Part B Eng. 164 (2019) 116–120.
[9] K. Gopalakrishnan, H. Ceylan, S. Kim, S. Yang, H. Abdualla, Electrically conductive mortar characterization for self-heating airfield concrete pavement mix design, Int. J. Pave. Res. Technol. 8 (5) (2015) 315–324.
[10] B. Suryanto, W.J. McCarter, G. Starrs, G.V. Ludford-Jones, Electrochemical immittance spectroscopy applied to a hybrid PVA/steel fiber engineered cementitious composite, Mater. Des. 105 (2016) 179–189.
[11] D. Wang, Q. Wang, Z. Huang, Investigation on the poor fluidity of electrically conductive cement-graphite paste: Experiment and simulation, Mater. Des. 169 (2019).
[12] S. Nayak, S. Das, Spatial damage sensing ability of metallic particulate-reinforced cementitious composites: Insights from electrical resistance tomography, Mater. Des. 175 (2019).
[13] P.T. Dalla, K.G. Dassios, I.K. Tragazikis, D.A. Exarchos, T.E. Matikas, Carbon nanotubes and nanofibers as strain and damage sensors for smart cement, Mater. Today Commun. 8 (2016) 196–204.
[14] P.-W. Chen, D. Chung, Concrete as a new strain/stress sensor, Compos. Part B Eng. 27 (1) (1996) 11–23.
[15] R. Howser, H. Dhonde, Y. Mo, Self-sensing of carbon nanofiber concrete columns subjected to reversed cyclic loading, Smart Mater. Struct. 20 (8) (2011).
[16] J. Gomis, O. Galao, V. Gomis, E. Zornoza, P. Garcés, Self-heating and deicing conductive cement. Experimental study and modeling, Constr. Build. Mater. 75 (2015) 442–449.
[17] S. Wen, D. Chung, Electromagnetic interference shielding reaching 70 dB in steel fiber cement, Cem. Concr. Res. 34 (2) (2004) 329–332.
[18] A. Sassani, H. Ceylan, S. Kim, K. Gopalakrishnan, A. Arabzadeh, P.C. Taylor, Influence of mix design variables on engineering properties of carbon fiber-modified electrically conductive concrete, Constr. Build. Mater. 152 (2017) 168–181.
[19] J. Wu, J. Liu, F. Yang, Three-phase composite conductive concrete for pavement deicing, Constr. Build. Mater. 75 (2015) 129–135.
[20] A. Arabzadeh, H. Ceylan, S. Kim, K. Gopalakrishnan, A. Sassani, S. Sundararajan, P.C. Taylor, Superhydrophobic coatings on Portland cement concrete surfaces, Constr. Build. Mater. 141 (2017) 393–401.
[21] A. Arabzadeh, H. Ceylan, et al. Influence of deicing salts on the water-repellency of Portland cement concrete coated with polytetrafluoroethylene and polyetheretherketone, in Airfield and Highway Pavements 2017, 2017, p. 217-227.
[22] H. Whittington, J. McCarter, M. Forde, The conduction of electricity through concrete, Magaz. Concr. Res. 33 (114) (1981) 48–60.
[23] A.S. El-Dieb, M.A. El-Ghareeb, M.A. Abdel-Rahman, A.N. El Sayed, Multifunctional electrically conductive concrete using different fillers, J. Build. Eng. 15 (2018) 61–69.
[24] Z. Tang, Z. Li, J. Qian, K. Wang, Experimental study on deicing performance of carbon fiber reinforced conductive concrete, J. Mater. Sci. Technol. 21 (1) (2005) 113–117.
[25] A. Peyvandi, P. Soroushian, A.M. Balachandra, K. Sobolev, Enhancement of the durability characteristics of concrete nanocomposite pipes with modified graphite nanoplatelets, Constr. Build. Mater. 47 (2013) 111–117.
[26] J. Cao, D. Chung, Carbon fiber reinforced cement mortar improved by using acrylic dispersion as an admixture, Cem. Concr. Res. 31 (11) (2001) 1633–1637.
[27] B. Chen, J. Liu, Effect of fibers on expansion of concrete with a large amount of high f-CaO fly ash, Cem. Concr. Res. 33 (10) (2003) 1549–1552.
[28] F. Xuli, D. Chung, Effect of methylcellulose admixture on the mechanical properties of cement, Cem. Concr. Res. 26 (4) (1996) 535–538.
[29] R. Polder, C. Andrade, et al., Test methods for on site measurement of resistivity of concrete, Mater. Struct. 33 (10) (2000) 603–611.
[30] H. Layssi, P. Ghods, A.R. Alizadeh, M. Salehi, Electrical resistivity of concrete, Concr. Int. 37 (5) (2015) 41–46.
[31] X. Tian, H. Hu, Test and study on electrical property of conductive concrete, Procedia Earth Planet. Sci. 5 (2012) 83–87.
[32] C.-T. Chen, J.-J. Chang, W.-C. Yeih, The effects of specimen parameters on the resistivity of concrete, Constr. Build. Mater. 71 (2014) 35–43.
[33] P. Ghosh, Q. Tran, Correlation between bulk and surface resistivity of concrete, Int. J. Concr. Struct. Mater. 9 (1) (2015) 119–132.
[34] H. Dehghanpour, K. Yilmaz, M. Ipek, Evaluation of recycled nano carbon black and waste erosion wires in electrically conductive concretes, Constr. Build. Mater. 221 (2019) 109–121.
[35] 802, T., Design of Concrete Mixes. 2016.
[36] T. Wu, R. Huang, M. Chi, T. Weng, A study on electrical and thermal properties of conductive concrete, Comput. Concr. 12 (3) (2013) 337–349.
[37] C. Chang, G. Song, D. Gao, Y. Mo, Temperature and mixing effects on electrical resistivity of carbon fiber enhanced concrete, Smart Mater. Struct. 22 (3) (2013).
[38] H. Dehghanpour, Synthesis and Characterization of Polypyrrole and Different Carbon Structures Based Nanocomposites for Supercapacitors, Fen Bilimleri Enstitüsü, Atatürk üniversitesi, Erzurum, 2015.

[39] H. Tang, X. Chen, Y. Luo, Electrical and dynamic mechanical behavior of carbon black filled polymer composites, Eur. Polym. J. 32 (8) (1996) 963–966.
[40] L. Shi, Y. Lu, Y. Bai, Mechanical and electrical characterisation of steel fiber and carbon black engineered cementitious composites, Procedia Eng. 188 (2017) 325–332.
[41] L. Rejon, A. Rosas-Zavala, J. Porcayo-Calderon, V. Castano, Percolation phenomena in carbon black–filled polymeric concrete, Polym. Eng. Sci. 40 (9) (2000) 2101–2104.
[42] Y. Ding, Z. Chen, Z. Han, Y. Zhang, F. Pacheco-Torgal, Nano-carbon black and carbon fiber as conductive materials for the diagnosing of the damage of concrete beam, Constr. Build. Mater. 43 (2013) 233–241.
[43] Z. Mikulova, I. Sedenkova, et al., Study of carbon black obtained by pyrolysis of waste scrap tyres, J. Therm. Analysis Calorimetry 111 (2) (2013) 1475–1481.
[44] M. Norouzi, Use of Nano Carbon Black in Mortar and the Effects of the Properties. Master's Thesis, 2016 Institute of Science, Ataturk University, Erzurum.
[45] R. Ram, M. Rahaman, A. Aldalbahi, D. Khastgir, Determination of percolation threshold and electrical conductivity of polyvinylidene fluoride (PVDF)/short carbon fiber (SCF) composites: effect of SCF aspect ratio, Polym. Int. 66 (4) (2017) 573–582.
[46] A. Belli, A. Mobili, T. Bellezze, F. Tittarelli, Commercial and recycled carbon/steel fibers for fiber-reinforced cement mortars with high electrical conductivity, Cem. Concr. Compos. 103569 (2020).
[47] W. Dong, W. Li, K. Wang, Z. Luo, D. Sheng, Self-sensing capabilities of cement-based sensor with layer-distributed conductive rubber fibres, Sens. Actuat. A Phys. 301 (2020).
[48] N. Anand, A. Godwin, Influence of mineral admixtures on mechanical properties of self-compacting concrete under elevated temperature, Fire Mater. 7 (40) (2016) 940–958.
[49] M. R. S. Wicaksono, A. Qoly, A. Hidayah, E.K. Pangestuti (2017, March). High stenghth concrete with high cement substitution by adding fly ash, CaCO3, silica sand, and superplasticizer, in: AIP Conference Proceedings (Vol. 1818, No. 1, p. 020068). AIP Publishing LLC.
[50] G.S. Rampradheep, M. Sivaraja, M. Geetha, R. Saranya, R. Sathish, V. Vignesh, M. Balaji, Exploration on micro structural and durability characteristics of Raphanussativus as an ingenious internal curing agent in concoction with self-compacting admixtures, Mater. Today Proc. 4 (10) (2017) 11088–11095.
[51] F. Xuli, D.D.L. Chung, Effect of methylcellulose admixture on the mechanical properties of cement, Cem. Concr. Res. 26 (4) (1996) 535–538.
[52] J. Cao, D.D.L. Chung, Carbon fiber reinforced cement mortar improved by using acrylic dispersion as an admixture, Cem. Concr. Res. 31 (11) (2001) 1633–1637.
[53] H. Dehghanpour, K. Yilmaz, Investigation of specimen size, geometry and temperature effects on resistivity of electrically conductive concretes, Constr. Build. Mater. 250 (2020).
[54] H. Dehghanpour, K. Yilmaz, The relationship between resistances measured by two-probe, Wenner probe and C1760-12 ASTM methods in electrically conductive concretes .SN Appl. Sci. 2 (1) (2020); 10.
[55] J. Yahaghi, Z.C. Muda, S.B. Beddu, Impact resistance of oil palm shells concrete reinforced with polypropylene fibre, Constr. Build. Mater. 123 (2016) 394–403.
[56] H. Dehghanpour, K. Yılmaz, Mechanical and Impact Behavior on Recycled Steel Fiber Reinforced Cementitious Mortars. Scientific Herald of the Voronezh State University of Architecture & Civil Engineering, 2018. 39(3).
[57] Y.A. Cengel, S. Klein, W. Beckman, Heat Transfer: A Practical Approach. Vol 141, (1998), McGraw-Hill New York.
[58] D. Systèmes, Abaqus 6.10: Analysis User Manual. Providence, RI: Dassault Systèmes Simulia Corp, 2010.
[59] S. Tungjitkusolmun, E. Woo, H. Cao, J. Tsai, V. Vorperian, J. Webster, Thermal—electrical finite element modelling for radio frequency cardiac ablation: effects of changes in myocardial properties, Med. Biol. Eng. Comput 38 (5) (2000) 562–568.
[60] Standared, A.S.T.M. D5334-14, Standard Test Method for Determination of Thermal Conductivity of Soil and Soft Rock by Thermal Needle Probe Procedure. ASTM International, West Conshohocken, PA (2014).
[61] P. Maleki, B. Iranpour, G. Shafabakhsh, Investigation of de-icing of roads with conductive concrete pavement containing carbon fibre-reinforced polymer (CFRP), Int. J. Pavement Eng. 20 (6) (2019) 682–690.
[62] S.S. Sadati, K.S Cetin, H. Ceylan, S. Kim, Energy-efficient design of a carbon fiber-based self-heating concrete pavement system through finite element analysis. Clean Technol. Environ. Policy, 1–11.
[63] M.A. Notani, A. Arabzadeh, H. Ceylan, S. Kim, K. Gopalakrishnan, Effect of carbon-fiber properties on volumetrics and ohmic heating of electrically conductive asphalt concrete, J. Mater. Civ. Eng. 31 (9) (2019) 04019200.
[64] S. Yehia, C.Y. Tuan, D. Ferdon, B. Chen, Conductive concrete overlay for bridge deck deicing: mixture proportioning, optimization, and properties, Mater. J. 97 (2) (2000) 172–181.
[65] C.Y. Tuan, Roca Spur Bridge: the implementation of an innovative deicing technology, J. Cold Regions Eng. 22 (1) (2008) 1–15.
[66] S. Yehia, C.Y. Tuan, Conductive concrete overlay for bridge deck deicing, Mater. J. 96 (3) (1999) 382–390.
[67] A. Sassani, H. Ceylan, S. Kim, A. Arabzadeh, P.C. Taylor, K. Gopalakrishnan, Development of carbon fiber-modified electrically conductive concrete for implementation in Des Moines International Airport, Case Stud. Constr. Mater. 8 (2018) 277–291.